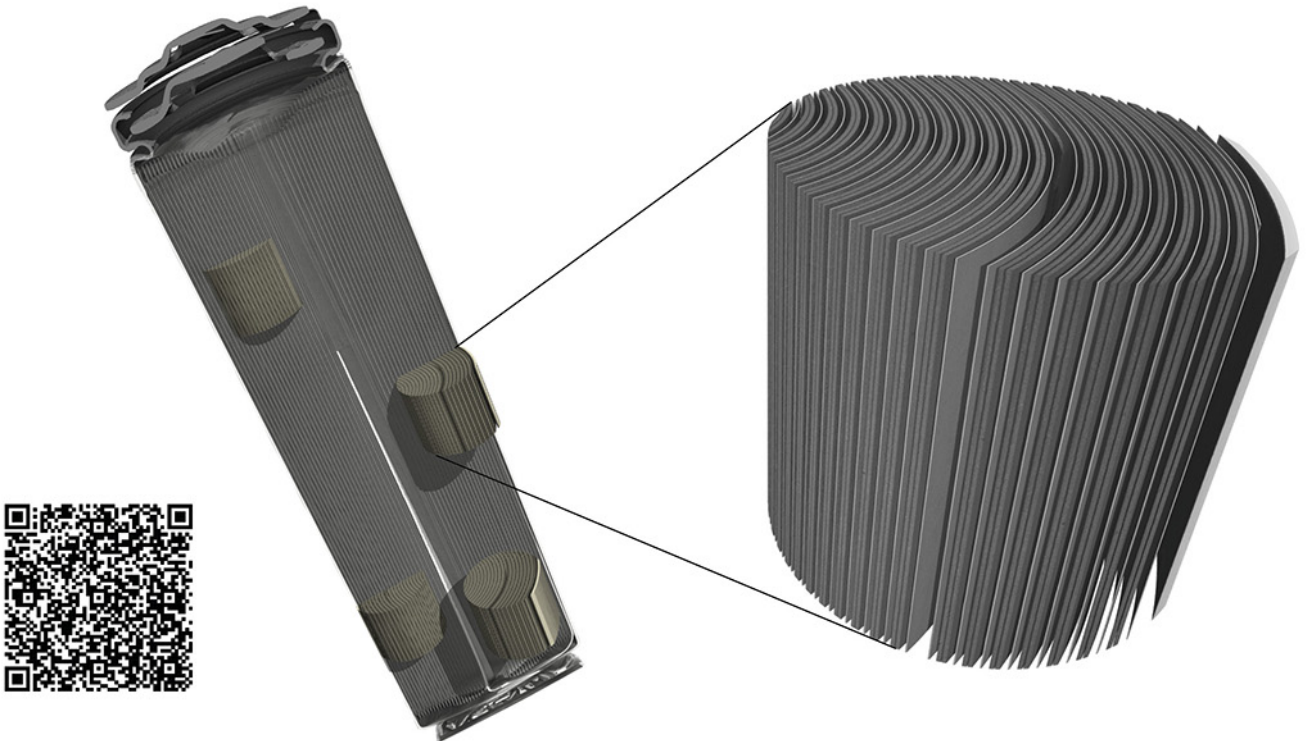


TESCAN micro-CT solutions

for energy storage materials research



TESCAN UniTOM XL

- ✓ Multi-scale non-destructive 3D imaging optimized to maximize throughput and contrast
- ✓ Fast scanning and high sample throughput with temporal resolutions below 10 seconds
- ✓ Wide array of samples types
- ✓ Enables dynamic tomography and *in-situ* experiments
- ✓ Dynamic screening for synchrotron beamtime
- ✓ Modular and open system with unmatched flexibility for research



[Click and find out more](#)

Water-Wave Driven Route Avoidance Warning System for Wireless Ocean Navigation

Zewei Ren, Xi Liang, Di Liu, Xunjia Li, Jianfeng Ping, Ziming Wang,
and Zhong Lin Wang*

The internet of things in the context of the ocean is vitally important. For ships sailing on the wide ocean in adverse weather conditions, evasion of marine islands and reefs is crucial to ensure safe navigation. Here, a hybrid wave energy harvesting nanogenerator is proposed (HW-NG) as a power source for long-distance wireless transmission, and demonstrated a self-powered route avoidance warning system for ocean navigation. The HW-NG is developed based on a triboelectric nanogenerator (TENG) and an electromagnetic generator (EMG), integrated by a pendulum structure. The TENG based on a contact-separation mode is designed into a spring-assisted multilayered structure, in which the EMG unit is well hybridized. Simply relying on the energy extracted from water waves, the HW-NG can establish long-distance (1.5 km) communication nodes on the sea. In application, a large HW-NG network could be developed in the adjacent water areas of islands or reefs. With a network formed by hundreds of thousands of HW-NGs, the forewarning signal transmission could be realized per second on the sea. More importantly, the wireless emitting is spontaneous through the designed automatic switch module. This work demonstrates a practicable strategy for ensuring safety of sea transportation based on wave energy collection.

meet big data transmission.^[1–3] Intelligent transportation system based on IoTs includes wireless sensor, telecommunication network, safe driving warning.^[4–7] For the overland traffic, the service is easy to be realized because of the strong power grid. However, the power supply of traffic warning system is limited on a vast sea area. Although some wireless warning devices like radio Aids-to-Navigation have been developed, they are generally powered by conventional batteries, which usually have limited lifetime and environmental issues.^[8–10] Since ocean occupies 70% of the earth surface area and wave energy distributes vastly in these water bodies, it is promising to utilize the water wave energy as sustainable power supply.^[11,12] Compared to other clean energy, water waves are also less affected by the alternating day and night as well as weather.^[13,14] However, the capture of wave energy and the development of self-

powered navigation warning system is still difficult, due to the current technology limitation.

Recently, the invention of triboelectric nanogenerator (TENG) has offered an unprecedented approach to collect environmental energy.^[15–17] Based on coupling effect of triboelectrification and electrostatic induction, the TENG devices perform well in low-frequency resources harvesting.^[18–22] Considering the massive amount on earth, the blue energy, which adopts TENG networks to collect wave energy, has been regarded as one of the major application fields of TENGs.^[23,24] Accordingly, a series of TENG prototypes have been developed targeting wave energy harvesting.^[25–30] Many kinds of novel materials and architectures are applied to these TENG prototypes,^[28–31] and small electronics such as light-emitting diode indicators, thermometers have been driven by the harvested energy.^[32,33] Although some wireless transmitters are also driven successfully by the TENG-based wave energy harvester, the transmission distance of which can only reach a few meters away.^[34,35] Furthermore, the power supply circuits of these wireless transmission is not automatic but manual, which make these reported demonstrations hard to achieve really application value.

In this work, a hybrid nanogenerator with TENG and electromagnetic generator (EMG) based on an optimized pendulum structure is reported to effectively harvest wave energy, used as

1. Introduction

With the development of Internet of Things (IoT), more and more wireless communication nodes need to be powered to

Dr. Z. Ren, Dr. X. Liang, D. Liu, Z. Wang, Prof. Z. L. Wang
CAS Center for Excellence in Nanoscience
Beijing Key Laboratory of Micro-nano Energy and Sensor
Beijing Institute of Nanoenergy and Nanosystems
Chinese Academy of Sciences
Beijing 100083, P. R. China
E-mail: zhong.wang@mse.gatech.edu

Dr. Z. Ren, Dr. X. Liang, D. Liu, Z. Wang, Prof. Z. L. Wang
School of Nanoscience and Technology
University of Chinese Academy of Sciences
Beijing 100049, P. R. China

X. Li, Prof. J. Ping
School of Biosystems Engineering and Food Science
Zhejiang University
866 Yuhangtang Road, Hangzhou 310058, P. R. China

Prof. Z. L. Wang
School of Material Science and Engineering
Georgia Institute of Technology
Atlanta, GA 30332-0245, USA

 The ORCID identification number(s) for the author(s) of this article can be found under <https://doi.org/10.1002/aenm.202101116>.

DOI: 10.1002/aenm.202101116

power source of a long-distance (1.5 km) wireless transmission. Accordingly, a self-powered route avoidance warning (RAW) system for ocean navigation is developed. The TENG utilizing the contact-separation mode is designed into a spring-assisted multilayered structure, where the EMG is well hybridized to fabricate the hybrid wave energy harvesting nanogenerator (HW-NG) device. The integration of TENG and EMG in the HW-NG can achieve their complementary strengths and enable the hybrid device to acquire satisfactory output over a broad range of operation frequency. By using the radio transmission with 433 MHz ultrahigh-frequency (Sub-1G), the long-distance (1.5 km) wireless communication nodes on the sea can be established with transmitting period less than a second, just relying on the energy extract from water waves with a large HW-NG network. More importantly, the signal emitting is automatically operated through the designed management circuit and voltage set of automatic switch module (ASM). In application, a self-powered navigation warning system consists of large HW-NG network can be developed in the adjacent water areas of islands or reefs, to ensure navigation safety of ships in all weather conditions.

2. Results and Discussion

2.1. Design and Operation of HW-NG

A schematic of HW-NG network distributing in the adjacent waters area of reefs for harvesting wave energy, and the developed automatic RAW system for ocean navigation is shown in **Figure 1a**. In bad weather and severe sea conditions like unforeseen fog or rainstorm, the visibility on the sea is very low for the sailing boats. The high-frequency warning information from HW-NG system can be timely captured by the terminal on the boats, and accordingly, the unsafe sailing route that likely to hit the reef would be avoided. **Figure 1b** illustrates structure of HW-NG device, where the composition can be divided into two parts: two multilayered TENGs, and one EMG unit with four copper (Cu) coils. Based on the single pendulum structure, the TENGs and EMG unit are effectively integrated. For each multilayered TENG, it's composed of six pairs of contact-separation mode TENGs (the enlarged view). Here, polyimide film (Kapton) is chosen as backbone of the multilayered TENG, due to its good mechanical strength and flexibility. The attached

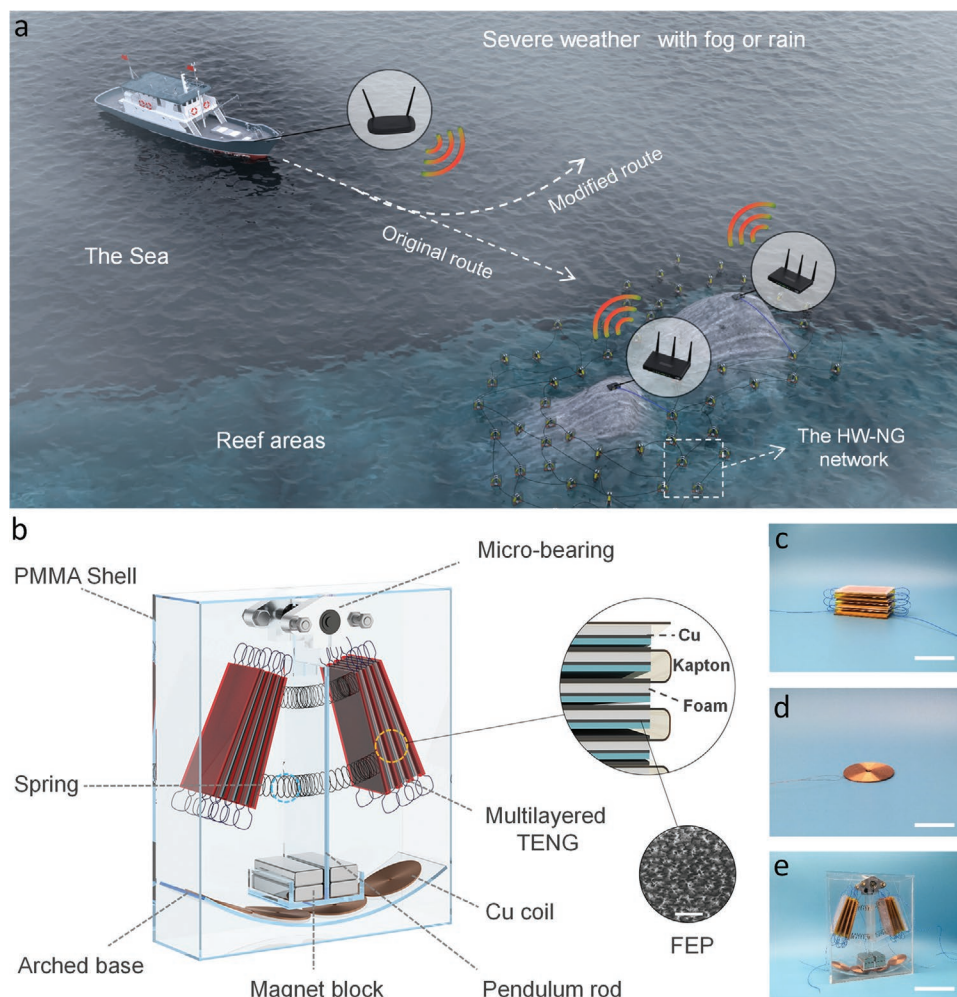


Figure 1. Design and operation of HW-NG. a). Schematic diagram of the self-powered automatic RAW system for ocean navigation based on HW-NG network. b). Structure and materials design of the HW-NG device, Scale bar in the SEM image is 2 μm . c–e). Photographs of the multilayered TENG, the Cu coil used by EMGs, and the HW-NG device, respectively. (Scale bar is 5, 3, and 7 cm, respectively).

Cu films have dual functions as positive tribo-layer of TENG and output electrode of negative tribo-layer. Fluorinated ethylene propylene (FEP) film is selected as dielectric material of negative tribo-layer because of its decent electron affinity. To enhance the charge density on the tribo-layer during contact electrification, nanostructure on surface of FEP has been developed by plasma etching, as scanning electron microscopy (SEM) image shown in the enlarged view. The wobbly magnet block and four Cu coils develop the EMG unit, realizing the maximized space utilization in one device. The magnet block there also plays the role of mass block to provide motion inertia for the pendulum. Since the motion trajectory of the wobbly magnet is arc, four Cu coils have been fixed on an arched polymethyl methacrylate (PMMA) base. Meanwhile, to enhance the contact of two tribo layers in the multilayered TENG tightly and avoid the excessive swing amplitude of the pendulum, the optimized springs have been fitted on two sides of the pendulum rod. Photographs of the multilayered TENG and Cu coil is presented in Figure 1c,d, respectively. Accordingly, the device is sealed by PMMA shells and forms the cuboid shape, as the photographs is shown in Figure 1e and Figure S1, Supporting Information.

The working principle of HW-NG for wave energy harvesting can be divided into two processes. That is, water wave drives HW-NG to roll, and then the swaying motion of pendulum rod generates electric output. The electrical energy is generated from two parts, one part from TENGs and another from EMG. The operation mechanism of TENG is based on coupling of contact electrification and electrostatic induction. With continuous swaying motion of the pendulum, a contact-separate motion between Cu and FEP tribo-layers would occur, leading to the changed electric potential difference between them. Accordingly, an alternating output can be induced in the external circuit, the detailed schematic of which can be found in Figure S2a, Supporting Information. The potential distribution in this process based on COMSOL simulation is depicted in Figure S2b, Supporting Information. Simultaneously, the electricity generation of EMG results from the magnetic flux's cutting by Cu coils. With the swing motion of magnet block that is attached to the bottom of pendulum rod, the magnets align and misalign with the Cu coils periodically, and then induces current in the coils. The output is then attained by the external circuit. The change of magnetic induction based on COMSOL simulation is presented in Figure S2c, Supporting Information.

2.2. Structure Design and Optimization of HW-NG

Since swaying motion of pendulum rod directly determines the out performance of HW-NG. The investigation of kinematic characteristics of simple pendulum and subsequent optimization is essential. That is, the output generated by the TENG and EMG units would all be enhanced, either with a larger swing amplitude or frequency of the pendulum. The detailed analysis can be found in Note S1, Supporting Information. For the pendulum in HW-NG device, the movement of which is an anharmonic damped motion. **Figure 2a** demonstrates the diagram of force distributed on the pendulum. Here, the length

of pendulum rod is defined as L , the mass of magnet block is m , and x presents the motion displacement when the swinging angle is θ . For the ideal simple pendulum without additional applied kinetic resistance, according to harmonic oscillator equation, the motion period of which can be deducted as:

$$T_0 = 2\pi \sqrt{\frac{L}{g}} \quad (1)$$

When swinging angle θ is large ($>5^\circ$), the damping period T of pendulum in arbitrary swinging angle can be modified as:

$$T = T_0 \left(\frac{\theta}{\sin \theta} \right)^{\frac{3}{8}} \quad (2)$$

The detailed derivation process can be found in Note S2, Supporting Information. For the pendulum rod in the HW-NG device, the influence of springs between the multilayered TENG and pendulum must be considered. As the mechanical model in Figure 2a shown, F_1 and F_2 present the forces that the springs applied on the rod, while F is pulling force along the rod. When the pendulum rod is static, the force state of magnet block can be derivate as:

$$F + 2kx \cos \beta = mg \quad (3)$$

In the circumstances, the equivalent gravitational acceleration is attained as:

$$g' = \frac{mg - 2kx \cos \beta}{m} \quad (4)$$

When the θ is small, the damping period T_0 in Equation (1) can be derivate as:

$$T_0 = 2\pi \sqrt{\frac{mL}{mg - 2kx \cos \beta}} \quad (5)$$

Further, based on the reduction of above basic model and Equation (2), the period T in arbitrary swinging angle can be acquired as:

$$T = 2\pi \sqrt{\frac{mL}{mg - 2kx \cos \beta}} \cdot \left(\frac{\theta}{\sin \theta} \right)^{\frac{3}{8}} \quad (6)$$

The details are expressed in Note S2, Supporting Information. Based on the above mechanical models, we can infer that if we want to acquire enhanced output from HW-NG under certain initial amplitude (external excitation), the period T should be as short as possible. Meanwhile, according to Equation (6), the deformation value of the spring between the multilayered TENG and pendulum rod should be 0, when the magnet mass remains relatively stationary in the initial equilibrium position. The axial direction of springs is supposed to be perpendicular to the contact-separation direction of the multilayered TENGs.

In addition, for the used springs there, several factors of these springs must be considered: stiffness coefficient, amount,

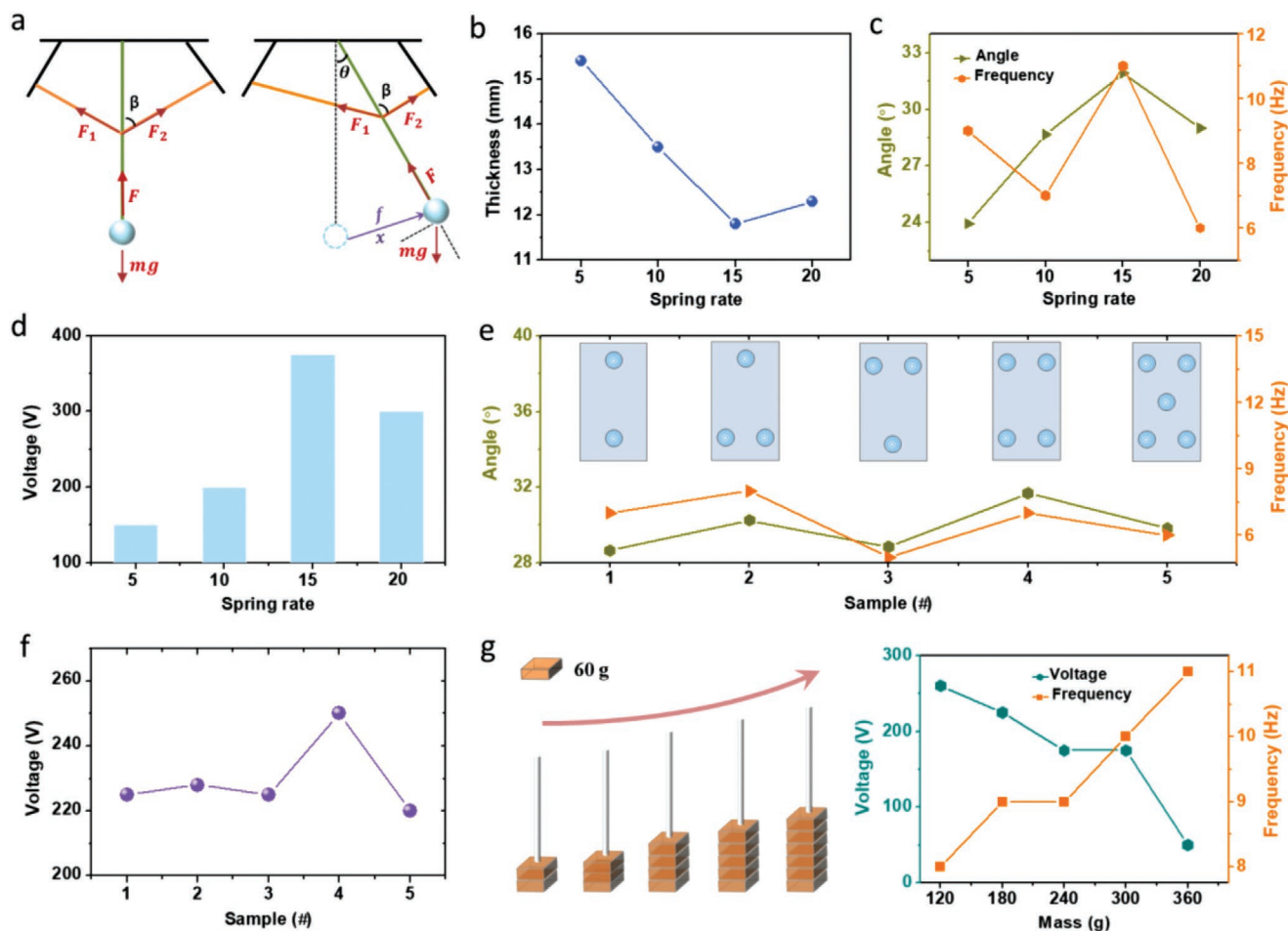


Figure 2. Kinematic characteristics and optimization of HW-NG. a). Schematic of force distributed on the pendulum for HW-NG. b). The compressed thickness of the multilayered TENG when the pendulum reaches maximum amplitude, under different coefficient springs. c). The pendulum's swing angle and frequency with different coefficient springs. d). The dependence of output on spring coefficient. e). The swing angle and frequency of pendulum and f) the output of HW-NG with distinct amount, distribution of springs. g) The influence of magnet block's mass on performance of HW-NG.

and their distribution. The influence of springs on swaying motion of pendulum is investigated (Figure 2b–f). It's noted that with the stiffness coefficient of 15, the pendulum's motion frequency and amplitude are both enhanced (Figure 2c). Here, the optimal value of the swing amplitude has also been implied by the compressed thickness of the multilayered TENG (Figure 2b and Figure S3, Supporting Information). In this way, the output performance of the TENG and EMG units would be both improved. Meanwhile, since the testing results demonstrate little relevance between the pendulum's swaying characteristics and the spring's amount or distribution (Figure 2e), the output fluctuation of both TENG and EMG units would be smooth. Take the TENG unit for example, the test has been carried out and the analysis is confirmed (Figure 2f).

Similarly, the influence of magnet block's mass on performance of HW-NG is studied. For the magnet block's mass (m), although the magnetic field would be enhanced with larger magnet block (larger mass), the swing amplitude of the pendulum must also be considered. Under a certain water wave, a larger m may weaken the swing amplitude of the pendulum. The detailed derivation and analysis are shown in Note S3,

Supporting Information. Hence, through the swing frequency increases slightly (from 8 to 11 Hz) when the mass of magnet block changing from 120 to 360 g (Figure 2g) and the magnetic field would be enhanced, the weight of magnet block can not be too large for ensuring the necessary swaying amplitude. Accordingly, the magnet blocks with mass of 240 g have been chosen.

2.3. Output Performance of HW-NG

Capability of the fabricated HW-NG for water wave energy harvesting is systematically studied, as presented in Figure 3. The typical power generation performances including open-circuit voltages (V_{OC}), short-circuit currents (I_{SC}), and output power are systematically measured. Here, to avoid the mismatched induction and interference in performance between the TENG and EMG, the output paths of the fabricated TENGs and EMG unit in the HW-NG device are separated. The optimal output of them can be acquired in their external load, respectively. In one HW-NG device, two multilayered TENGs are connected

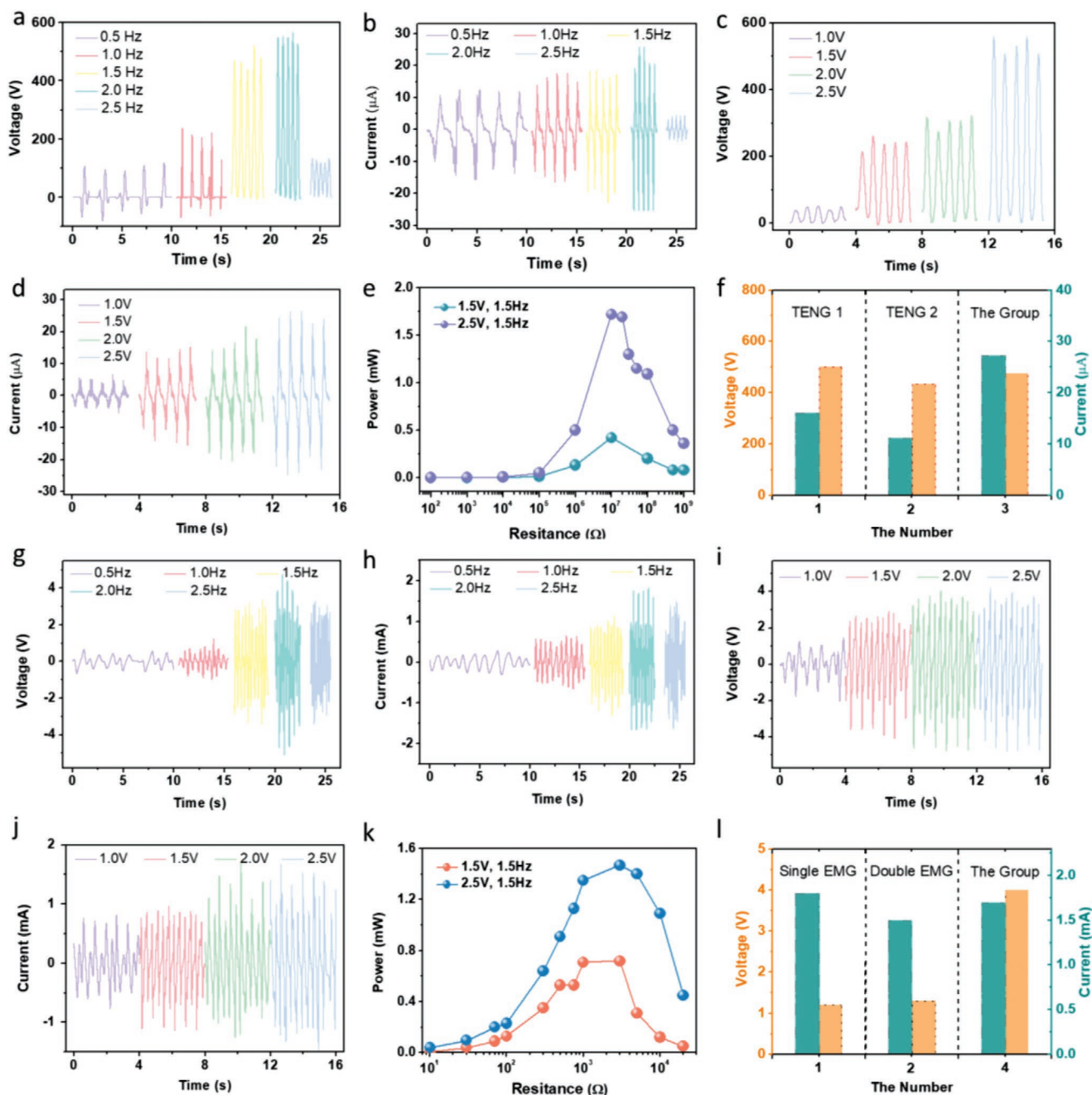


Figure 3. Electrical characteristics of the single HW-NG device. a–d). Outputs of V_{OC} and I_{SC} induced by TENG unit when a,b) wave frequency ranging from 0.5–2.5 Hz, c,d) H_{out} ranging from 1.0–2.5 V. e). The instantaneous output power of the TENG unit with different external load. f). The outputs of two TENGs before and after united to one TENG unit. g–j). Outputs of V_{OC} and I_{SC} induced by EMG unit when g,h) wave frequency ranging from 0.5–2.5 Hz, i,j) H_{out} ranging from 1.0–2.5 V. k). The instantaneous output power of the EMG unit with different external load. l). Output performance variation of the EMG fabricated by different number of Cu coils.

in parallel forming one output unit. As shown in Figure 3a,b, the dependence of output V_{OC} and I_{SC} of the TENG unit on the water wave frequency (0.5–2.5 Hz) has been measured, where the voltage amplitude of the function generator H_{out} is 2.5 V. The H_{out} value there is adopted to reflect amplitude of water waves, since an approximately proportional relationship exists between it and wave amplitude. It's noted that with increasing wave frequency, the V_{OC} and I_{SC} both first increase and then

decrease. The maximum output values of 580 V and 28 μ A are acquired when the frequency is around 2.0 Hz. The decreased output with higher frequency may attribute to the sufficient press of the multilayered TENGs, resulting from the reduced vibration period of pendulum. Figure 3c,d exhibit the influence of the wave amplitude H_{out} on the outputs of TENG unit. At the optimal frequency of 1.5 Hz, the outputs (V_{OC} and I_{SC}) are positively correlated with the H_{out} . That is, a larger water wave

amplitude is more beneficial to the operation of the TENG. The reason for this change is mainly because the TENG can't be fully driven by slight waves at small amplitude due to the device's weight. The instantaneous outputs of the TENG unit with different external load is shown in Figure S4a,b, Supporting Information and Figure 3e. With the matched resistance of $10\text{ M}\Omega$, the output power reaches 1.72 mW and power density reaches 0.41 W m^{-2} when the parameters of water wave are 2.5 V (H_{out}) and 1.5 Hz (frequency). Meanwhile, to testify effectiveness of circuit-level parallel strategies of two multilayered TENGs in the device, outputs of two TENGs before and after united are tested (Figure 3f). The results have elaborated the good usability of the integrated output path. The durability of multilayered TENG unit when the HW-NG operated at high water wave frequency is also tested (Figure S5, Supporting Information). The output of the TENG unit and operation state of HW-NG device perform stable with no apparent fluctuation, after 130 000 continuous working cycles.

Figure 3g,h demonstrate the outputs of the EMG unit at water wave frequency from 0.5 to 2.5 Hz (H_{out} is set as 2.5 V). Similarly, with the increasing wave frequency, the outputs of EMG unit also exhibit the change in arc curve. Although the output I_{SC} of EMG is several orders of magnitude larger than that of TENG, the V_{OC} is very small. At the frequency of 2.0 Hz , a maximum instantaneous output of 4.5 V and 1.5 mA is acquired. When wave frequency beyond 2.0 Hz , the failing of outputs may be caused by the decreased amplitude of pendulum. The relationship between the outputs of EMG unit and H_{out} has been given in Figure 3i,j, where the higher wave intensity in favor of the performance of EMG. Figure 3k illustrates instantaneous output power of the EMG unit under various external load, while the V_{OC} and I_{SC} can be found in Figure S4c,d, Supporting Information. At the wave frequency of 1.5 Hz and amplitude of 2.5 V , an instantaneous power of 1.48 mW and power density of 0.30 W m^{-2} are attained under matching resistance of $2\text{ K}\Omega$. The influence of the magnet-coil pair number on the EMG's performance is also studied, indicating that the output can be raised by increasing the number of Cu coil (Figure 3l).

2.4. Performance of HW-NG Network Array

For realizing large-scale wave energy harvesting in the wide ocean, the research on TENG network is essential. In a single HW-NG device, all of the basic units are able to move synchronously, because of the unified swing of the device. Nevertheless, the full realization of motion phase sameness in the HW-NG array is difficult, due to the different motion states of HW-NG under the water wave movements. To achieve effective construction of network and acquire optimum output performance, the HW-NG units must be connected through mutually independent rectifier bridges. In this case, the energy harvested by HW-NG network would not offset. Here, an HW-NG network array with four HW-NG units linked by span wires is fabricated and experimented. In one HW-NG device, the rectification of TENG and EMG units are segregated to avoid mutual interference. Each TENG or EMG unit is first connected to a rectifier bridge respectively, and at the same time, the output

from them is converted to DC output. Schematic of the connection circuit between the rectifier bridges and TENGs in the HW-NG network is shown in Figure 4a, where all the TENGs are connected in parallel. Differently, all the EMGs in the HW-NG network have been series-connected, as the schematic shown in Figure 4d. In the four HW-NG network, the output performance of TENG and EMG units network after rectification under different wave intensity are systematically studied, as shown in Figures 4b,c and 4e,f, respectively. Under the wave intensity of 2.5 V (H_{out}) and 1.5 Hz (frequency), the output generated by TENG network is around 600 V and $90\text{ }\mu\text{A}$, while the EMG network reaches around 11 V and 1.6 mA . The results illustrate the effectiveness of the integrated TENG and EMG units in the HW-NG network array. The testing experimental photographs can be found in Figure 4g and Figure S6, Supporting Information, where the HW-NG network is driven by water wave in a wave-simulation water tank.

To meet the electricity demands of subsequent applications, the charging performances of single HW-NG device and four-HW-NG network to load capacitors are investigated, respectively. Figure 4h shows the charging voltage curves for different capacitors by a single HW-NG, under the water wave of 2.5 V (H_{out}) and 1.5 Hz (frequency). For capacitors with different capacities, the charging speeds of which are all fast at the beginning and then trend to smooth. A higher charging speed would be got with the smaller capacitance. For capacitors with capacitance of 0.47 and 79 mF , the charging voltage can respectively reach 3.1 and 1.8 V within 60 s . However, the charging of capacities would be limited when the charging voltage reaches saturation. In this stage, although the charging power source (the single HW-NG) is operated normally, voltage value of the capacitor cannot continue to increase (as the curves in Figure 4h show). That's because the leakage of the capacitor is more significant in this large-voltage stage, the electricity induced by the single HW-NG is unable to surpass the leakage at the time. With the HW-NG network fabricated by a series of HW-NGs, the relation between the induced electricity and leakage of capacitors can be broken. Figure 4i exhibits the charging curves of the same capacitors by the four-HW-NGs network, under the same wave conditions. It's noted that charging speed and saturated voltage value of the capacitor are improved effectively. With charging time of 60 s , the voltages of the capacitor of 0.47 mF can reach 4.3 V , while the voltage near saturation with value of 5.6 V . Moreover, it's found that for the capacitor beyond 3.3 mF , the charging voltage of which is more resistant to saturation. Meanwhile, the charging speed can still retain a high value when the smaller capacitors nearly steady, which is an encouraging phenomenon and demonstrating the powerful power supply capability of HW-NG network.

2.5. RAW System for Ocean Navigation

Based on the powerful wave energy harvesting capability of HW-NG network, a self-powered RAW system for ocean navigation on the sea can be developed. Here, the navigation warning system is experimentally tested and demonstrated, as shown in Figure 5. To achieve the long-distance wireless transmission, the wireless network nodes controller of ultra-low power

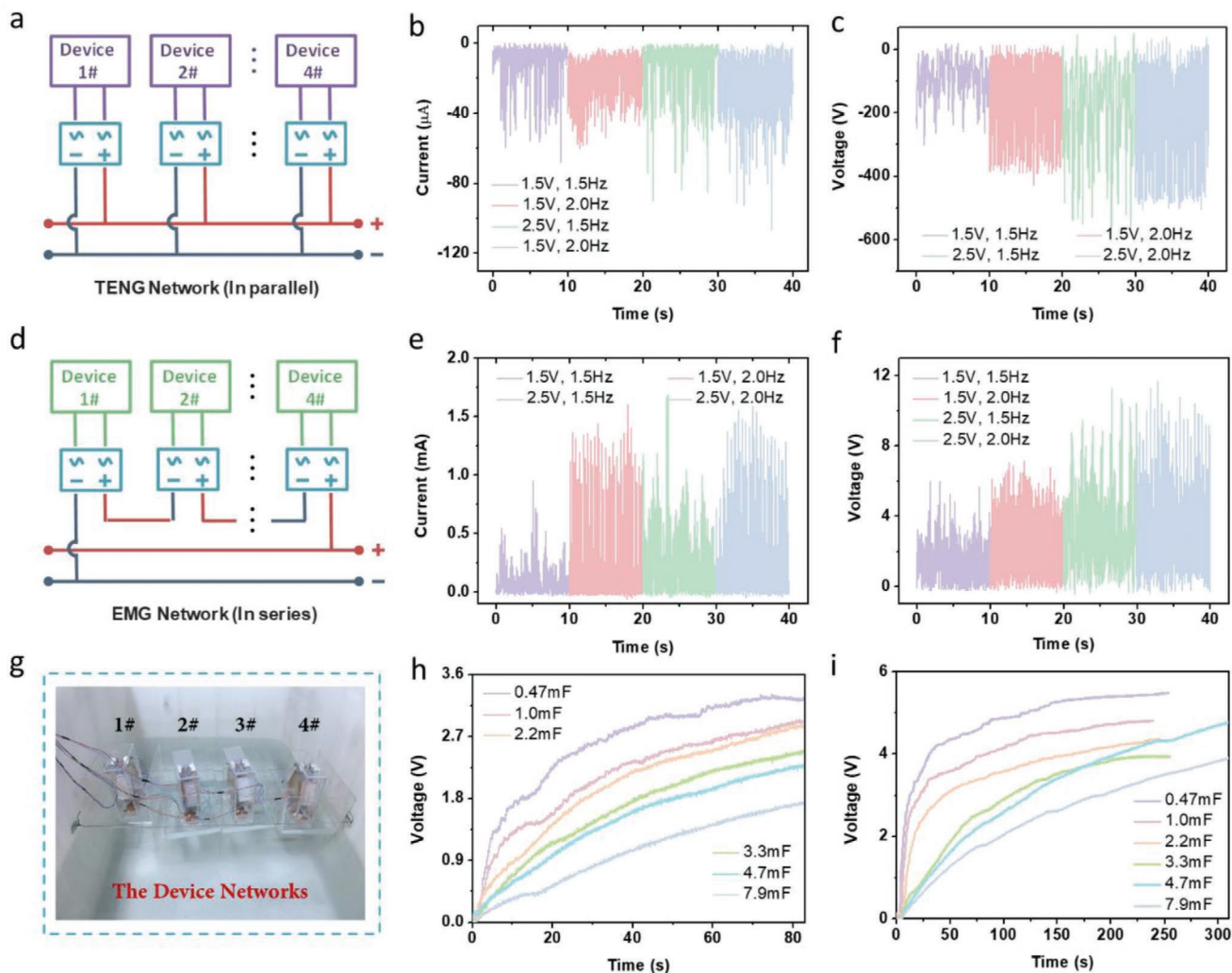


Figure 4. Output performance of HW-NG network. a). Schematic of the connection circuit between the rectifier bridges and TENG units in the HW-NG network. b,c). Outputs of TENG network under different wave frequency and amplitude conditions. d). Schematic of the connection circuit between the rectifier bridges and EMG units in the HW-NG network. e,f). Outputs of EMG network under different wave frequency and amplitude conditions. g). The testing experimental photographs of the four-HW-NG network. h,i). Charging voltage curves for different capacitors by h) a single HW-NG and i) the four-HW-NG network.

is designed, as shown in Figure 5a. On the ocean, the transmitter is totally supplied by HW-NG network, the core modules of which including a Sub-1G module and the main processor of CC1310. For improving the quality of signal transmission, a rod antenna is installed there. Figure 5b shows the designed ASM based on power management circuit, which can intellectually control open of the power source. The open voltage of ASM can be set from 3 to 4 V, while the off voltage is around 2.2 V. The working circuit of the self-powered navigation warning system is shown in Figure 5c. Firstly, the electricity generated by the HW-NG network stores in the capacitor. When the capacitor voltage reaches the set value of 3.4 V, the ASM is open and then the electricity in the capacitor releases, until the capacitor voltage down to 2.2 V the switch is off. The whole process is operated automatically. In this process, the released electricity from the capacitor would supply the transmitter and send out the warning signals. Demonstration of the self-powered RAW

system for ocean navigation can be found in Figure 5d,e and Video S1, Supporting Information. When the capacitor of 9.4 mF is charged from 0 to 3.4 V around 5 min by the four HW-NGs network, the system is activated. The enlarged circuit of transmitting node of the system can be found in Figure S7, Supporting Information. Correspondingly, we have developed a RAW app installed on the mobile phone, where the RAW is connected with the wireless terminal via Bluetooth. In application, when the boats on the sea sail into the safe distance around the reefs, they will receive the RAW signals and the RAW can give an alarm intuitively (as change shown in Figure 5e and Figure S8, Supporting Information). The voltage variation of the capacitor in warning system for two consequent transmitting processes is exhibited in Figure 5f. Figure 5g demonstrates the current change of the wireless transmitter when it's worked, the current sharply change to 20 mA when the signals are transmitted. Meanwhile, the transmitting distance between

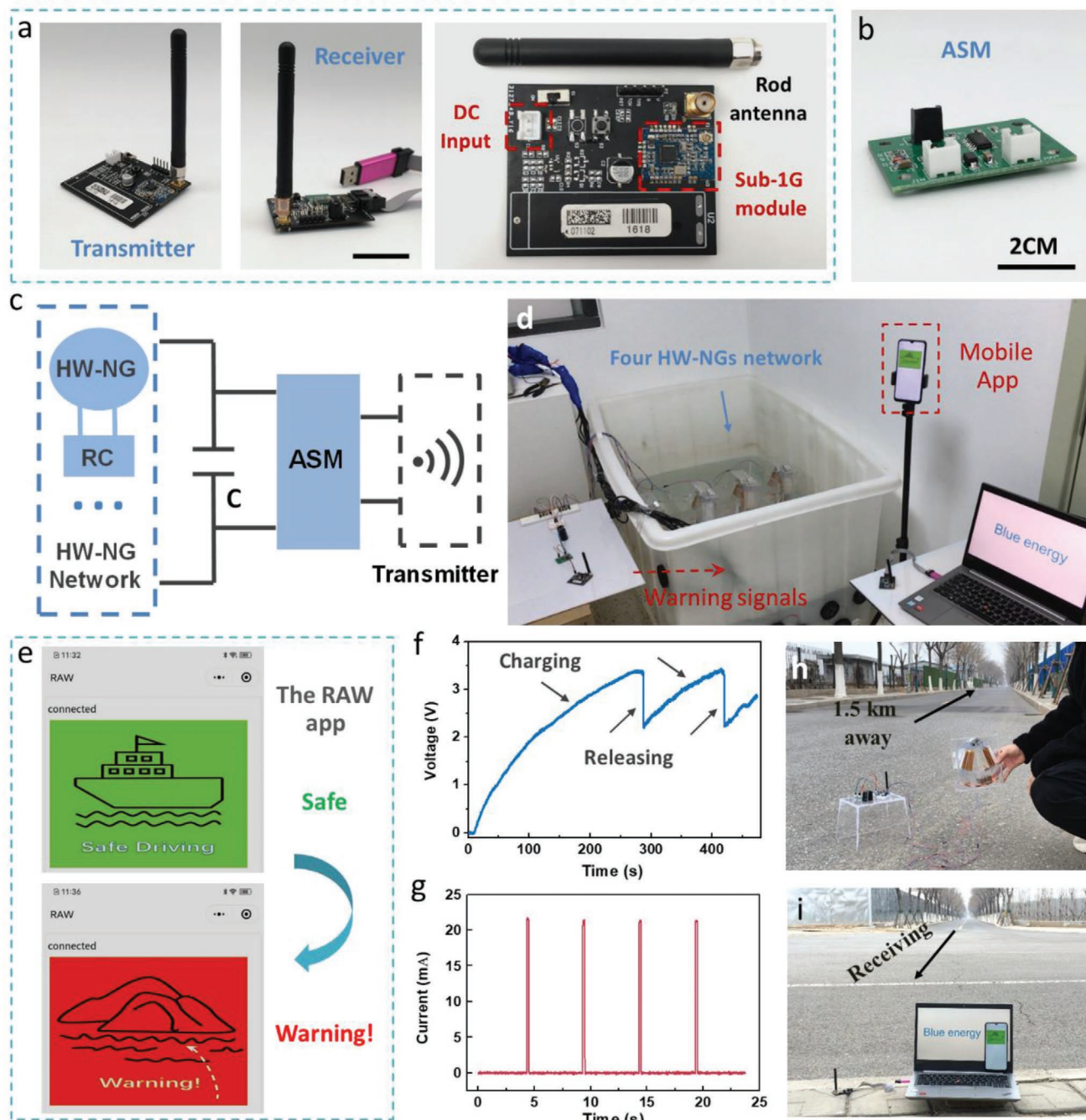


Figure 5. Illustration of the self-powered RAW system for ocean navigation. a) Photographs and illustrations of the long-distance wireless modules. b) Photograph of the ASM. c) Circuit schematic of the self-powered RAW system. d) Demonstration of the warning system for ocean navigation. e) The enlarged view of change of the RAW app installed on mobile phone. f) Voltage variation of the capacitor (9.4 mF) in consequent wireless transmission processes. g) The current change of the wireless transmitter when it's worked. h,i) The distance test experiment of the communication nodes outdoors.

our communication nodes has also been actually tested outdoors, as shown in Figure 5h,i and Figure S9 and Video S2, Supporting Information. The test is carried out along a straight road (Figure S9a, Supporting Information). In this testing, an HW-NG device is shaken to charge the capacitor and supply the transmitter (Figure 5h and Figure S9b, Supporting Information). The stable transmitting distance between the transmitter and receiver is demonstrated as far as 1.5 km, as shown

in Figure S9c,d and Video S2, Supporting Information. Since charging speed of the capacitor in the system depends on the HW-NG network, the automatic emission interval of warning signal can be changed by adjusting amount of HW-NGs in the network. Based on the experimental four HW-NGs network, it's estimated that with the network consist of 600 HW-NGs, the signal transmitting period is less than a second. With the larger network array distributed on the water areas around marine

islands and reefs, the interval can be shorter and realize real-time traffic warning for the sailing ships.

3. Conclusion

In summary, an HW-NG device based on TENG and EMG technologies has been proposed, used as power source of long-distance (1.5 km as of now) communication nodes on the sea. Based on the HW-NG network, a self-powered RAW system for ocean navigation has been developed, which can provide safety warning for sailing boats. The TENG and EMG units are integrated in the HW-NG device by an optimized pendulum structure, in which wave energy can be effectively collected by swing of the pendulum. The integration of TENG and EMG can achieve their complementary strengths and enable the hybrid device to acquire satisfactory output over a broad range of operation frequency. In the adjacent waters area of islands or reefs, with an integrated HW-NG network formed by hundreds of thousands of HW-NGs, the warning signal can be transmitted in real-time. Meanwhile, the wireless transmission is spontaneous, with assistance of the designed ASM based on power management circuit. This work may provide a practicable strategy for developing traffic warning system of marine transportation by utilizing blue energy.

4. Experimental Section

Fabrication of the Multilayered TENG: The Kapton film (thickness of 50 μm) with size of 32 cm \times 7 cm was chosen to serve as the substrate of the multilayered TENG. Then the Kapton strip was folded into eight squares (7 cm \times 4 cm) and shaped into a zigzag structure. The Cu foil (7 cm \times 4 cm) and an FEP film (thickness of 12.5 μm , size of 7 cm \times 4 cm) bonded by another Cu foil (6 cm \times 3.5 cm) were adhered on two adjacent intervals of the Kapton strip. The surface of FEP film was carried out with hydrophobic treatment with hydrophobic agent (combination of nano silicon dioxide, ethanol, and organosilicon resin), to enhance the triboelectrification. The surface between Kapton and Cu coil of FEP-Cu film was attached by a flexible foam (7 cm \times 4 cm), since the contact between two tribo layers can be improved.

Fabrication of the HW-NG Device: The PMMA plates (thickness of 4 cm) were selected as shell of HW-NG, while the pendulum bar was also fabricated by acrylic blocks. The rotation axle of the pendulum was fixed on the PMMA shell by a miniature bearing and screws. The swing diameter was the pendulum around 16 cm, where the wobbly magnet block with mass of 240 g was attached to the bottom of the pendulum. Two multilayered TENGs were fabricated on both sides of the pendulum, and acrylic substrates were adopted to support them. The four Cu coils of EMG unit were fixed on the arched PMMA base, where the diameters of the used Cu coils are 4 cm (outer diameter) and 4.2 mm (internal diameter). The thickness of the coil is 1 mm, and the coil turns was around 1200. The diameter of the wire that was used to fabricate the coils is 0.08 mm. The vertical distance between the middle Cu coil and the wobbly magnet block is around 1 cm. Accordingly, the whole HW-NG device was sealed and waterproof treatment.

Characterization and Measurement: Microstructure of the FEP film was acquired by using SEM (SU8020, Hitachi). The wave-simulation water tank was composed of eight wave-making pumps (rw-20 Jpower Technology Inc.), where the pumps were unified controlled by a function generator (AFG3011C Tektronix Inc.). Videos and photographs were captured by camera (Canon 600D, Japan) and high-speed camera (Photron, Japan). The electrical output without rectification was measured by Stanford Research Systems Keithley 6514. After

rectification, the current was measured by Keithley 6514 while the voltage was measured by the digital oscilloscope (Agilent InfiniiVision 2000X).

Supporting Information

Supporting Information is available from the Wiley Online Library or from the author.

Acknowledgements

The research was supported by the National Key R & D Project from Minister of Science and Technology (2016YFA0202704), National Natural Science Foundation of China (Grant Nos. 51605033, 51432005, 5151101243, 51561145021), Beijing Municipal Science and Technology Commission (Z171100000317001, Z171100002017017, Y3993113DF). The authors declare that they have no competing interests.

Conflict of Interest

The authors declare no conflict of interest.

Data Availability Statement

Research data are not shared.

Keywords

traffic warnings, triboelectric nanogenerators, wave energy harvesting, wireless ocean navigation

Received: April 7, 2021

Revised: June 5, 2021

Published online:

- [1] R. Haight, W. Haensch, D. Friedman, *Science* **2016**, 353, 124.
- [2] V. Marx, *Nature* **2013**, 498, 255.
- [3] K. Pan, Y. Fan, T. Leng, J. Li, Z. Xin, J. Zhang, L. Hao, J. Gallop, K. S. Novoselov, Z. Hu, *Nat. Commun.* **2018**, 9, 5197.
- [4] J. A. Guerrero-ibanez, S. Zeadally, J. Contreras-Castillo, *IEEE Wireless Communications* **2015**, 22, 122.
- [5] H. Zhou, B. Li, D. Wang, *Internet of Things* **2102**, 312, 572.
- [6] L. D. Xu, W. He, S. Li, *IEEE Transactions on Industrial Informatics* **2014**, 10, 2233.
- [7] J. A. Stankovic, *IEEE Internet of Things Journal* **2014**, 1, 3.
- [8] H. Chen, F. Yin, W. Huang, M. Liu, D. Li, *Sensors* **2020**, 20, 2598.
- [9] A. E. Pallares-Calvo, B. E. Carvajal-Gómez, O. O. Gutiérrez-Frías, *Emerging Imaging and Sensing Technologies for Security and Defence III; and Unmanned Sensors, Systems, and Countermeasures*, SPIE, Bellingham, WA **2018**.
- [10] L. C. Langebrake, C. E. Lembke, R. H. Weisberg, R. H. Byrnes, D. R. Russell, G. Tilbury, R. Carr, *OCEANS '02 MTS/IEEE* **2002**, 1, 98.
- [11] S. P. Beeby, R. N. Torah, M. J. Tudor, P. Glynne-Jones, T. O.' Donnell, C. R. Saha, S. Roy, *J. Micromech. Microeng.* **2007**, 17, 1257.
- [12] Z. L. Wang, J. Chen, L. Lin, *Energy Environ. Sci.* **2015**, 8, 2250.
- [13] Y. Bai, L. Xu, C. He, L. Zhu, X. Yang, T. Jiang, W. Zhong, J. Nie, Z. L. Wang, *Nano Energy* **2019**, 66, 104117.

- [14] F. D. O. Antonio, *Renewable Sustainable Energy Rev.* **2010**, *14*, 899.
- [15] F. Fan, Z. Tian, Z. L. Wang, *Nano Energy* **2012**, *1*, 328.
- [16] Z. L. Wang, *ACS Nano* **2013**, *7*, 9533.
- [17] Z. Ren, Y. Ding, J. Nie, F. Wang, L. Xu, S. Lin, X. Chen, Z. L. Wang, *ACS Appl. Mater. Interfaces* **2019**, *11*, 6143.
- [18] J. Zhu, M. Zhu, Q. Shi, F. Wen, L. Liu, B. Dong, A. Haroun, Y. Yang, P. Vachon, X. Guo, T. He, C. Lee, *EcoMat* **2020**, *2*, e12058.
- [19] H. Guo, X. He, J. Zhong, Q. Zhong, Q. Leng, C. Hu, J. Chen, L. Tian, Y. Xia, J. Zhou, *J. Mater. Chem. A* **2014**, *2*, 2079.
- [20] Y. Zi, L. Lin, J. Wang, S. Wang, J. Chen, X. Fan, P. Yang, F. Yi, Z. L. Wang, *Adv. Mater.* **2015**, *27*, 2340.
- [21] Z. Ren, Z. Wang, Z. Liu, L. Wang, H. Guo, L. Li, S. Li, X. Chen, W. Tang, Z. L. Wang, *Adv. Energy Mater.* **2020**, *10*, 2001770.
- [22] Q. Shi, Z. Sun, Z. Zhang, C. Lee, *Research* **2021**, *2021*, 6849171.
- [23] J. Tollefson, *Nature* **2014**, *508*, 302.
- [24] Z. L. Wang, *Nature* **2017**, *542*, 159.
- [25] Y. Pang, S. Chen, Y. Chu, Z. L. Wang, C. Cao, *Nano Energy* **2019**, *66*, 104131.
- [26] X. Wang, S. Niu, Y. Yin, F. Yi, Z. You, Z. L. Wang, *Adv. Energy Mater.* **2015**, *5*, 1501467.
- [27] L. Liu, Q. Shi, C. Lee, *Nano Energy* **2020**, *76*, 105052.
- [28] Z. H. Lin, G. Cheng, L. Lin, S. Lee, Z. L. Wang, *Angew. Chem., Int. Ed.* **2013**, *52*, 12545.
- [29] L. Liu, Q. Shi, J. S. Ho, C. Lee, *Nano Energy* **2019**, *66*, 104167.
- [30] T. Jiang, L. Zhang, X. Chen, C. Han, W. Tang, C. Zhang, L. Xu, Z. L. Wang, *ACS Nano* **2015**, *9*, 12562.
- [31] C. Hou, T. Chen, Y. Li, M. Huang, Q. Shi, H. Liu, L. Sun, C. Lee, *Nano Energy* **2019**, *63*, 103871.
- [32] W. Zhong, L. Xu, X. Yang, W. Tang, J. Shao, B. Chen, Z. L. Wang, *Nanoscale* **2019**, *11*, 7199.
- [33] K. Lee, J. Lee, K. Kim, D. Yoo, D. S. Kim, W. Hwang, I. Song, J. Y. Sim, *Micromachines* **2018**, *9*, 598.
- [34] J. An, Z. Wang, T. Jiang, X. Liang, Z. L. Wang, *Adv. Funct. Mater.* **2019**, *29*, 1904867.
- [35] X. J. Zhao, S. Y. Kuang, Z. L. Wang, G. Zhu, *ACS Nano* **2018**, *12*, 4280.